ADVANCED HEALTHCARE MATERIALS

Supporting Information

for *Adv. Healthcare Mater.*, DOI 10.1002/adhm.202401783

Biocompatibility of Water-Dispersible Pristine Graphene and Graphene Oxide Using a Close-to-Human Animal Model: A Pilot Study on Swine

Paola Nicolussi, Giovannantonio Pilo, Maria Giovanna Cancedda, Guotao Peng, Ngoc Do Quyen Chau, Alejandro De la Cadena, Renzo Vanna, Yarjan Abdul Samad, Tanweer Ahmed, Jeremia Marcellino, Giuseppe Tedde, Linda Giro, Acelya Ylmazer, Federica Loi, Gavina Carta, Loredana Secchi, Silvia Dei Giudici, Simona Macciocu, Dario Polli, Yuta Nishina, Ciriaco Ligios, Giulio Cerullo, Andrea Ferrari, Alberto Bianco, Bengt Fadeel, Giulia Franzoni and Lucia Gemma Delogu**

Supporting Information

Biocompatibility of water-dispersible pristine graphene and graphene oxide using a close-to-human animal model: a pilot study on swine

Paola Nicolussi[1], Giovannantonio Pilo[1], Maria Giovanna Cancedda[1], Guotao Peng[2], Ngoc Do Quyen Chau[3], Alejandro De La Cadena Perez Gallardo[4], Renzo Vanna[5], Yarjan Abdul Samad[6,7], Tanweer Ahmed[6], Jeremia Marcellino[6], Giuseppe Tedde[1], Linda Giro[8], Acelya Ylmazer[9], Federica Loi[1], Gavina Carta[1], Loredana Secchi[1], Silvia Dei Giudici[1], Simona Macciocu[1], Dario Polli[4,5], Yuta Nishina[10,11], Ciriaco Ligios[1], Giulio Cerullo[4,5], Andrea Ferrari[6], Alberto Bianco[3], Bengt Fadeel[2], Giulia Franzoni[1]* and Lucia Gemma Delogu[8]*

(1) Istituto Zooprofilattico Sperimentale della Sardegna, Sassari, Italy
(2) Institute of Environmental Medicine, Karolinska Institutet, Stockholm, Sweden
(3) CNRS, Immunology, Immunopathology and Therapeutic Chemistry, UPR 3572, University of Strasbourg ISIS, 67000 Strasbourg, France
(4) Dipartimento di Fisica, Politecnico di Milano, Milan, Italy
(5) Istituto di Fotonica e Nanotecnologie - CNR, Milan, Italy
(6) Cambridge Graphene Centre, University of Cambridge, Cambridge, United Kingdom
(7) Department of Aerospace Engineering, Khalifa University of Science & Technology, UAE
(8) ImmuneNano Laboratory, Department of Biomedical Sciences, University of Padua, Padua, Italy
(9) Department of Biomedical Engineering, Ankara University, Ankara, Turkey
(10) Graduate School of Natural Science and Technology, Okayama University, Tsushimanaka, Kita-ku, Okayama, 700-8530, Japan
(11) Research Core for Interdisciplinary Sciences, Okayama University, Tsushimanaka, Kita-ku, Okayama, 700-8530, Japan

*Corresponding authors: luciagemma.delogu@unipd.it, giulia.franzoni@izs-sardegna.it

Running title: No toxicity of graphene in a porcine model.

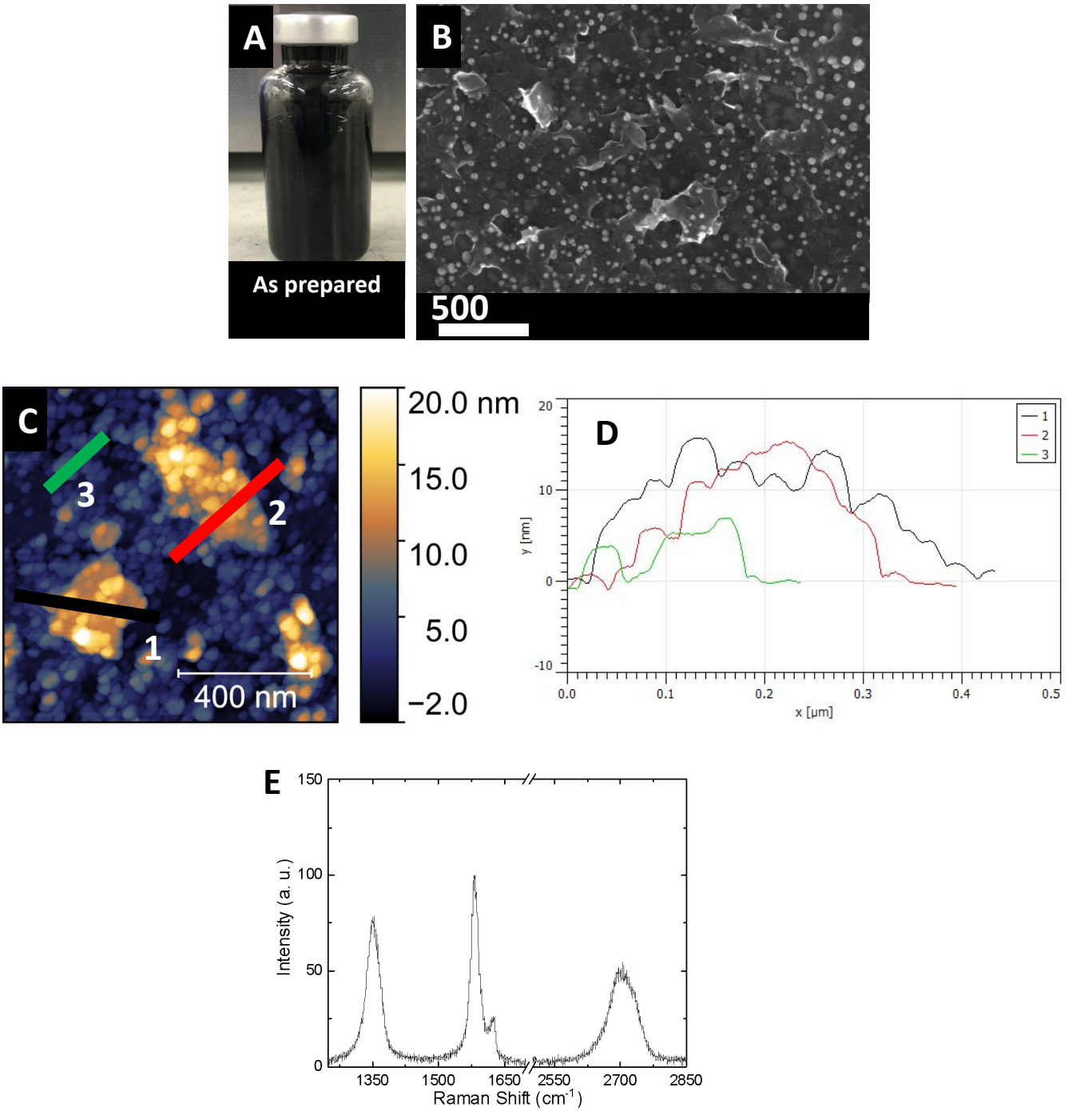

Figure S1. Pristine graphene characterization. A) As prepared pristine graphene (GR). B) SEM image of GR-FBS dispersion C) AFM image and D) thickness measurements of graphene flakes. E) Raman spectrum of GR.

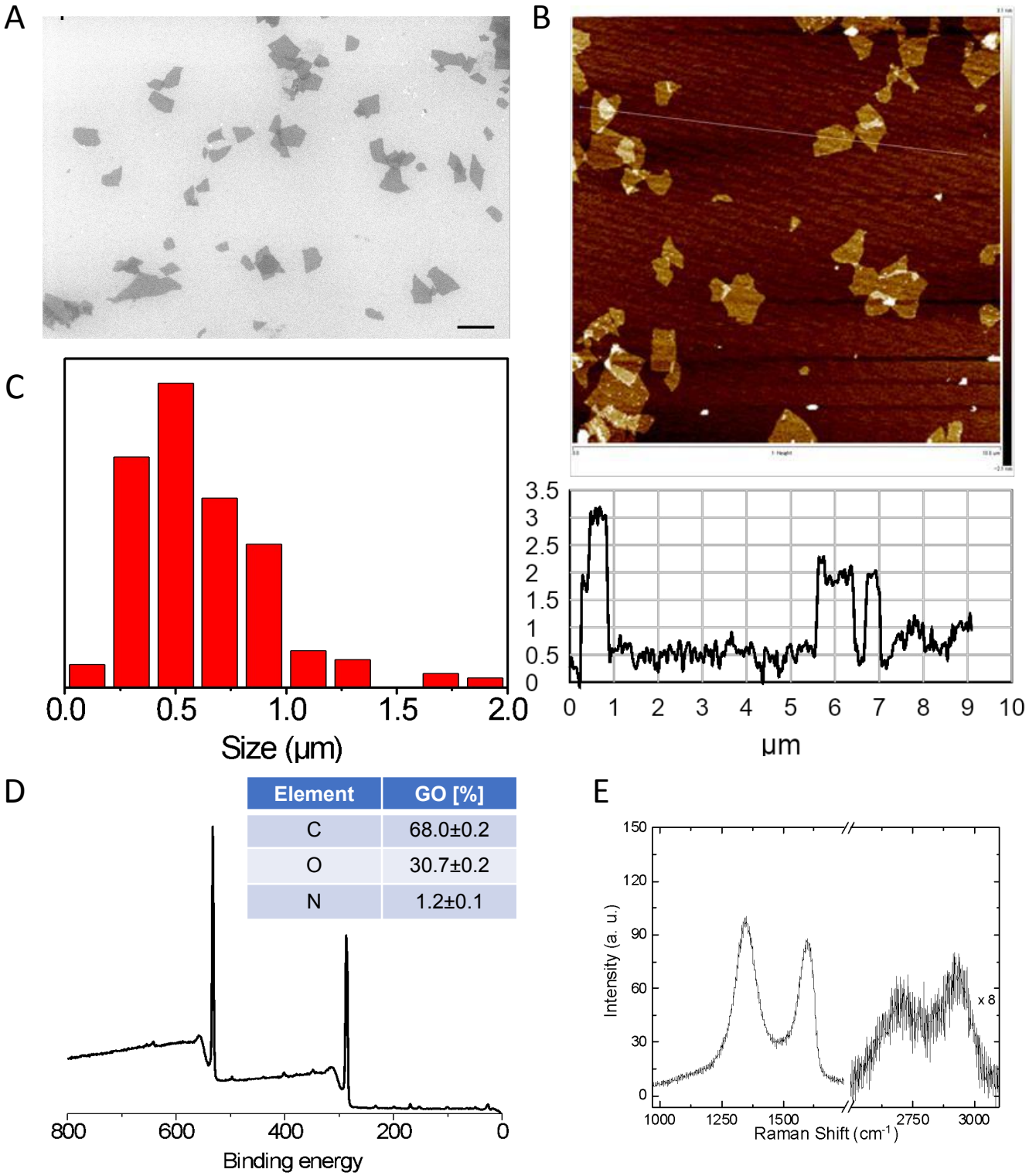

Figure S2. Graphene oxide characterization. A) SEM of single layer GO sheets. B) AFM images of GO sheets. C) Lateral size distribution was calculated from SEM images by measuring more than 200 sheets. D) XPS survey spectrum. E) Raman spectrum of GO.

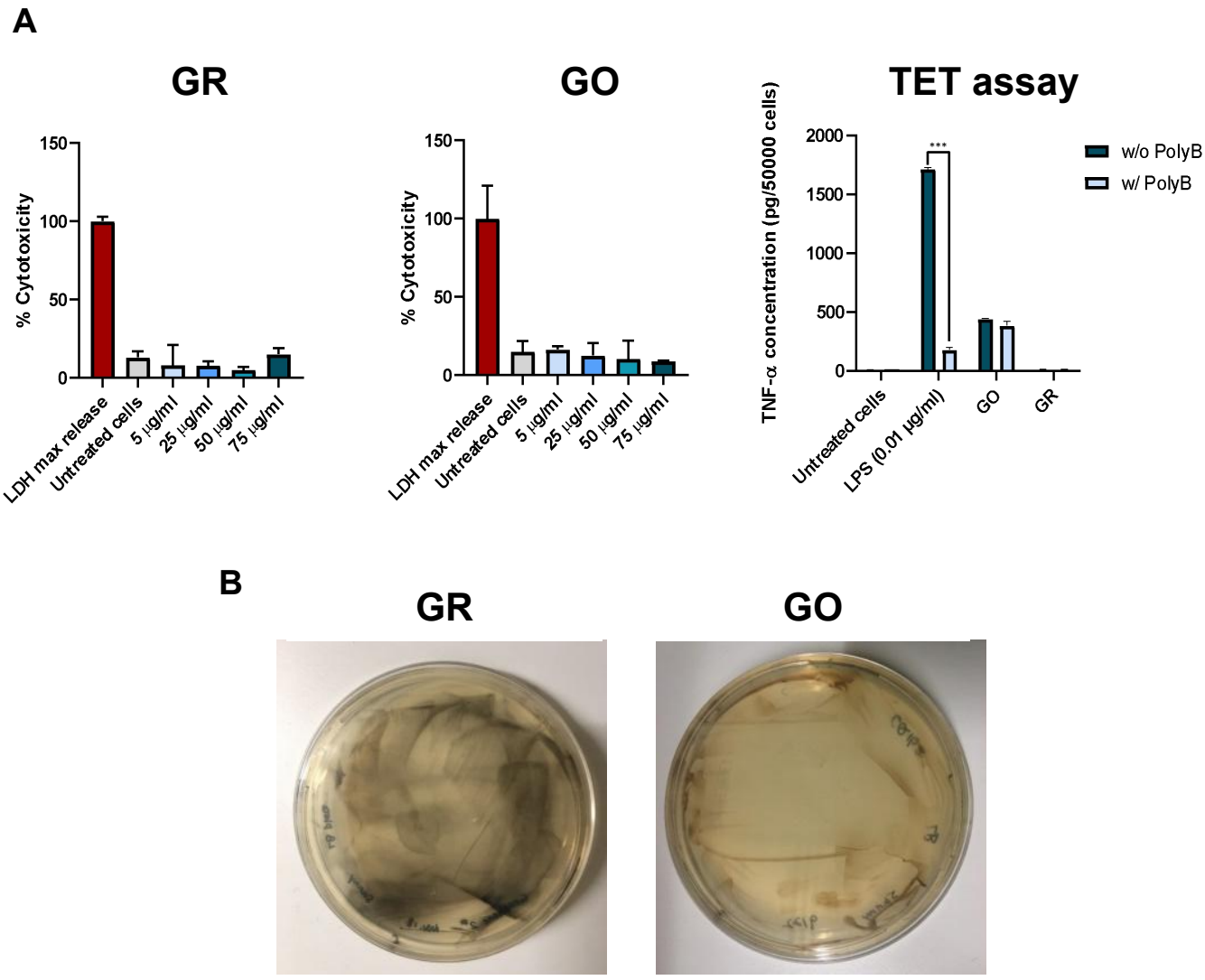

Figure S3. Endotoxin content and sterility of GR and GO. A) Endotoxin content of GR and GO. First, cell viability was assessed on HMDMs following GR or GO exposure. Cells were exposed to GR and GO at different concentrations (5, 25, 50, 75 μg/mL) for 24 h and then cell viability was assessed by the LDH release assay. Then, TET was performed to detect endotoxin content in GR and GO using a non-toxic dose (25 μg/mL). The presence of Poly-B (10 μM) significantly blocked LPS-triggered TNF-α expression. B) Sterility test was performed by plating GR or GO suspensions on LB agar plates and incubating them overnight at 37°C. No bacterial colonies were formed after incubation.

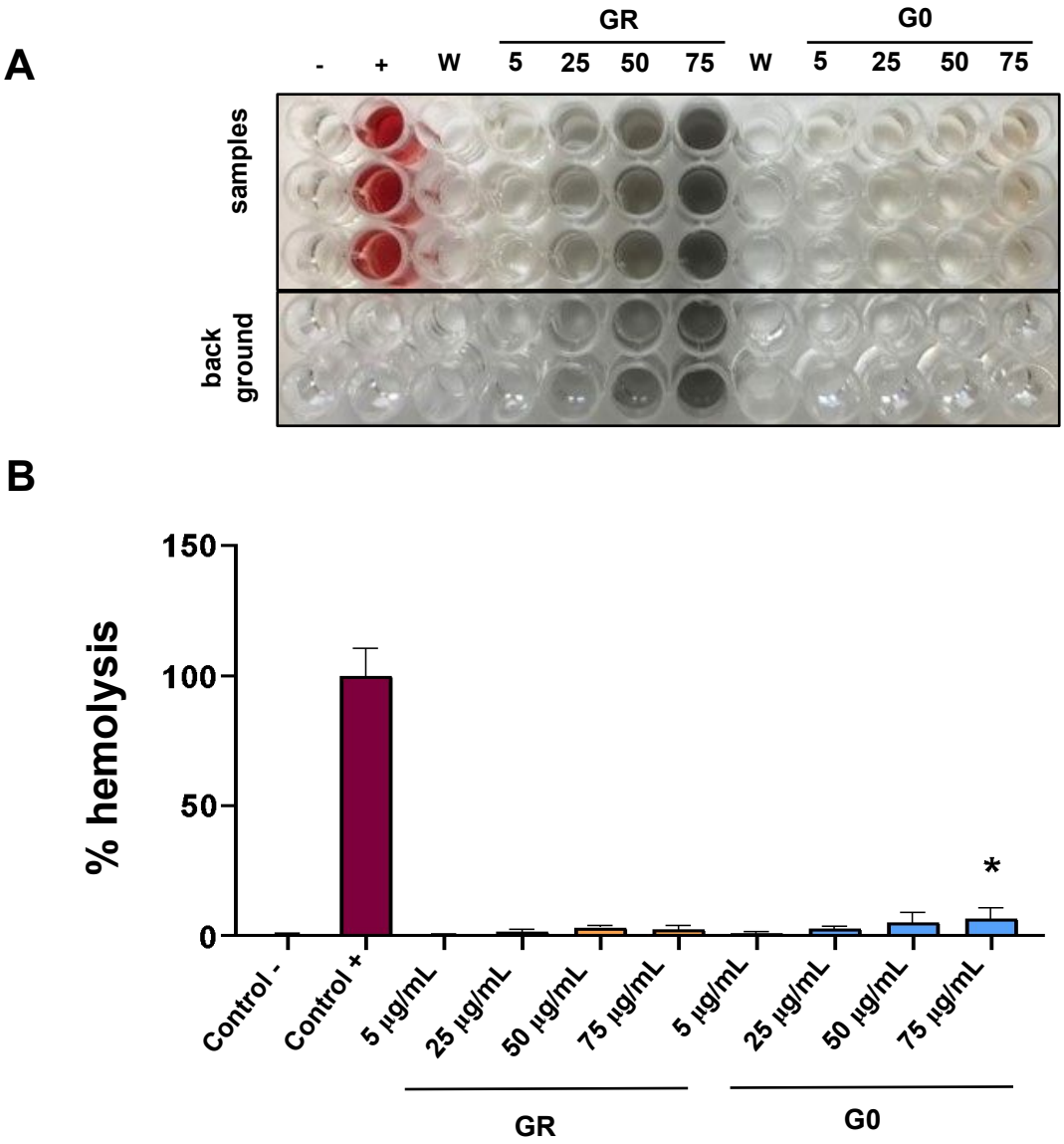

Figure S4. Hemocompatibility of GR and GO. GR or GO were incubated at increasing concentrations (5, 25, 50, 75 µg/mL) for 24 h with swine RBCs. The absorbance of hemoglobin release in the supernatant was read at 570 nm. Pictures of supernatants of RBCs treated with different GBMs are displayed. The red color of the solution is due to the release of hemoglobin from damaged RBCs. RBCs incubated with isotonic PBS and RBCs incubated with deionized water were used as positive and negative controls, respectively. PBS incubated with increasing concentration of GBMs without RBCs was used as additional control (background). Background values were subtracted from values of GBM-treated RBCs. GBM-treated samples were then compared to the corresponding untreated control (Control -) using a one-way ANOVA followed by a Bonferroni's multiple comparison test. *$p<0.05$.

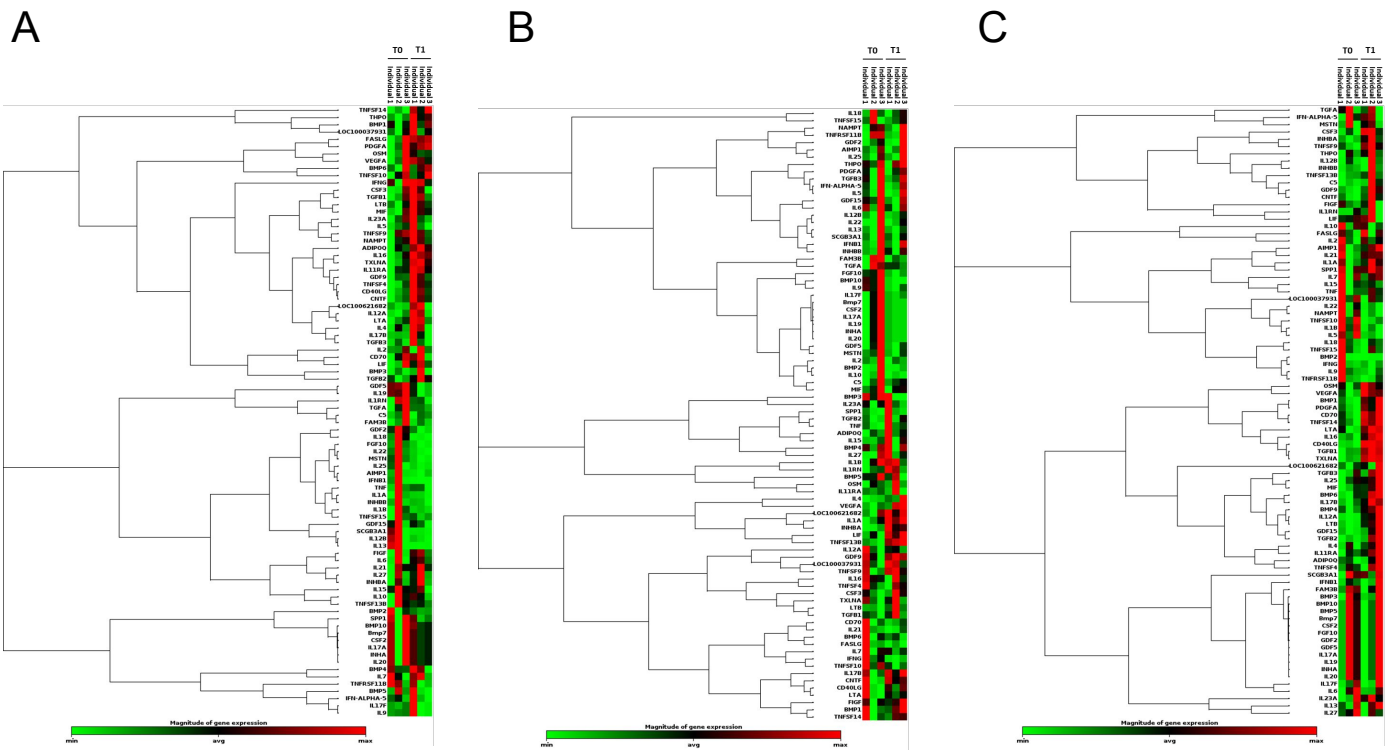

Figure S5. PBMC gene expression 24 h post administration of GR or GO. Pigs were injected intra-peritoneal with 15 mg of GR or GO or water, all with glucose (final glucose 5% w/v). Pre-injection (T_0) and after 24 h (T_1) EDTA blood was collected, PBMCs purified, RNA extracted and gene expression was carried out on three pigs per group. A, B, C) Non-supervised hierarchical clustering analysis of 84 gene expression pattern in each individual within the groups: control (A), GR (B) and GO (C). The colors in the cells represent the relative magnitude of gene expression. The black color represents the average magnitude of gene expression. The brightest green represents the smallest value, and the brightest red represents the highest value.

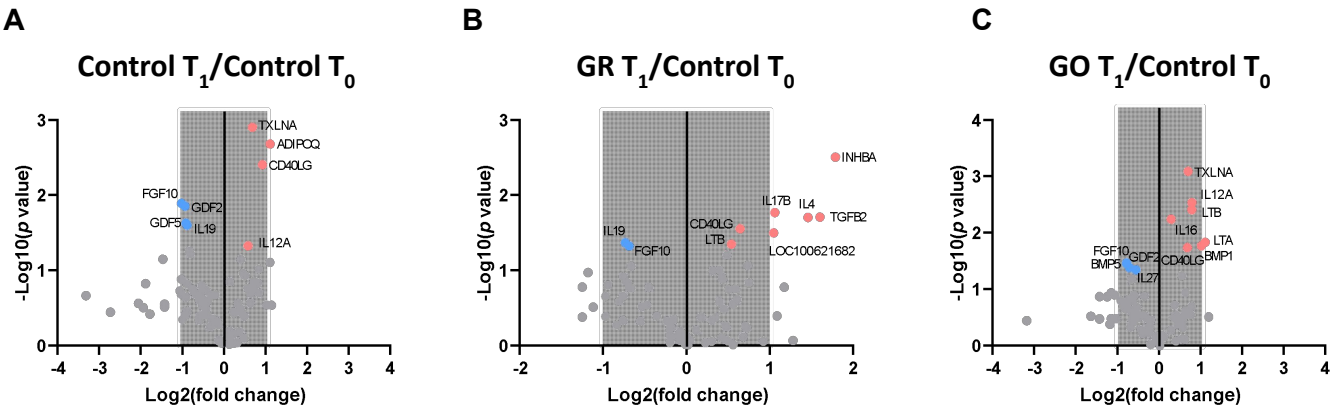

Figure S6. PBMC gene expression 24 h post administration of GR or GO. Pigs were injected intra-peritoneal with 15 mg of GR or GO or water, all with glucose (final glucose 5% w/v). Pre-injection (T_0) and after 24 h (T_1) EDTA blood was collected, PBMCs purified, RNA extracted and gene expression was carried out on three pigs per group. Three volcano plots show the 84 genes expression at T_1 in control, GR and GO groups compared to T_0 in control. T_0 was presented as the average of nine individuals. Significantly up- and down-regulated genes were marked in red and blue, respectively. Genes plotted farther from the central axis have larger changes in gene expression. Thresholds of 2-fold change were indicated in the shadow. The statistically significant difference was set as $p < 0.05$.

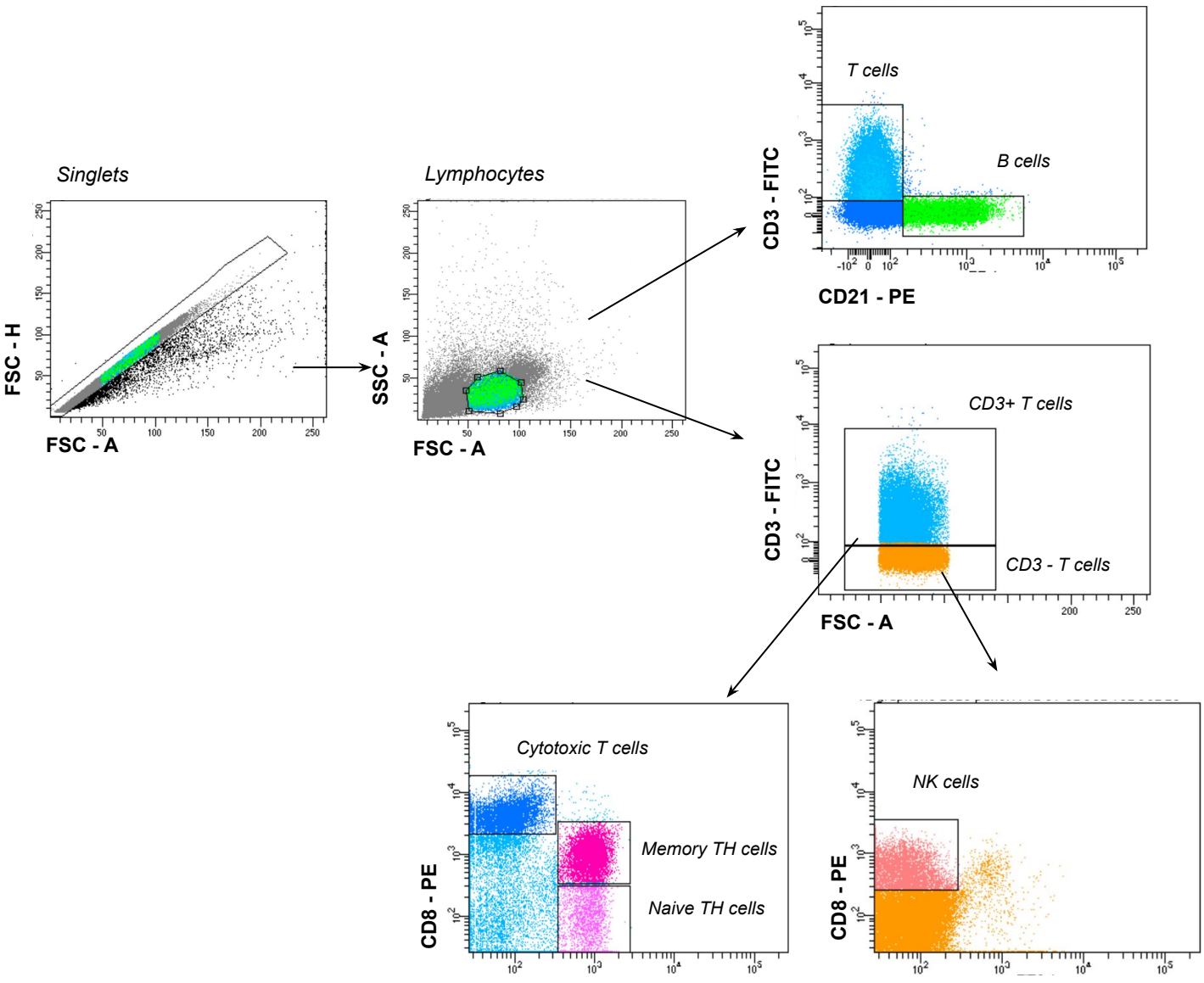

Figure S7. Gating strategy to evaluated changes in lymphocyte subsets in vivo. PBMCs were purified from EDTA blood and then different lymphocyte populations were discriminated using flow cytometry. Singlets lymphocytes were analyzed. Changes in different lymphocyte populations (B cells, T cells, NK cells) were assessed, as well as variation in different T cell populations (Cytotoxic T cells $CD8^{high}CD4^{-}$, Memory Th cells $CD8^{+}CD4^{+}$, Naïve Th cells $CD8^{-}CD4^{+}$).

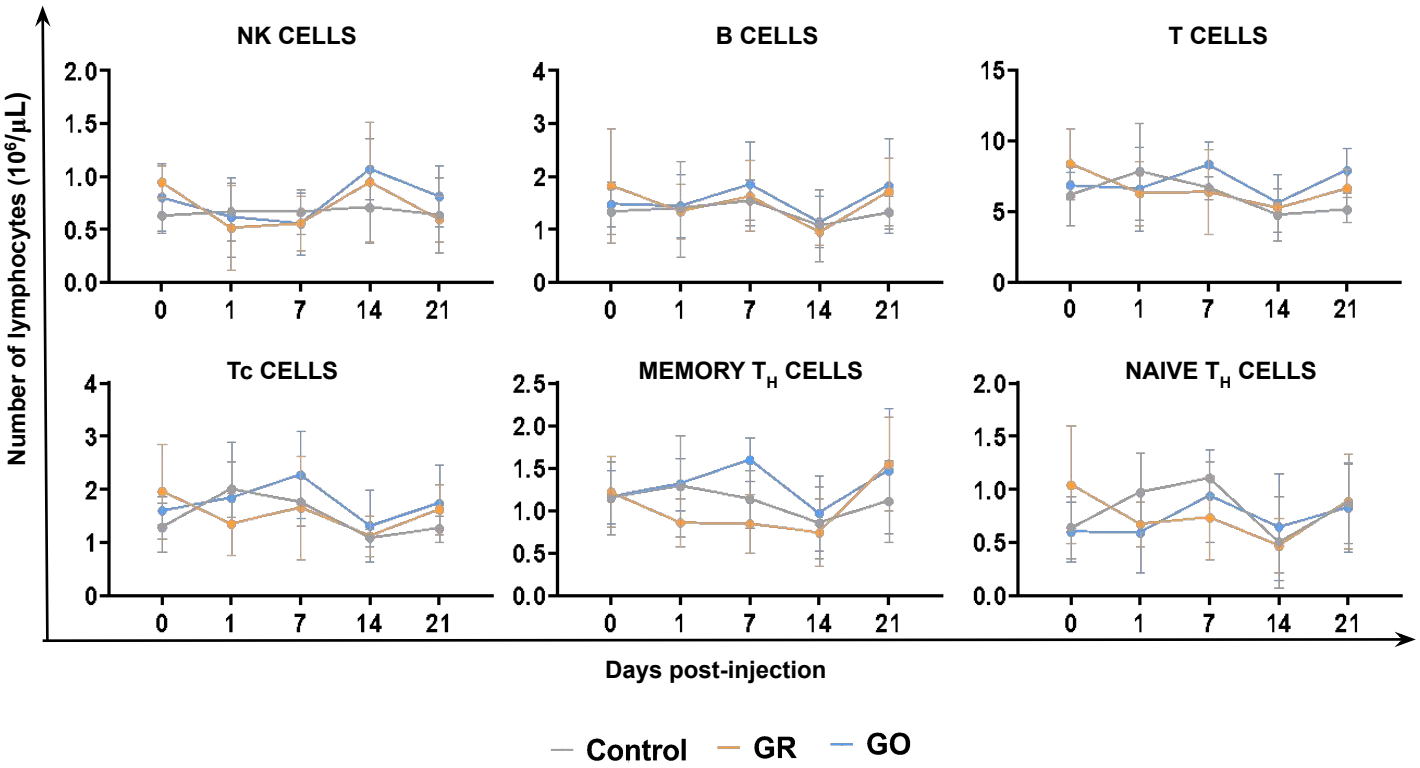

Figure S8. Changes in lymphocyte subsets in vivo after GR or GO injection. Pigs were injected intra-peritoneal with 15 mg of GR or GO or water, all with glucose (final glucose 5% w/v). Pre-injection (0) and after 1, 7, 14, 21 days blood was collected. EDTA blood was collected to perform complete blood counts and to purify PBMCs, then different lymphocyte populations were discriminated using flow cytometry. Changes in different lymphocyte populations (B cells, T cells, NK cells) were assessed, as well as variation in different T cell populations (Cytotoxic T cells, Memory Th cells, Naïve Th cells). Data from three controls or five treated different pigs are presented as mean + SD. At each time post-injection, values were compared using a one-way ANOVA followed by a Bonferroni's multiple comparison test.

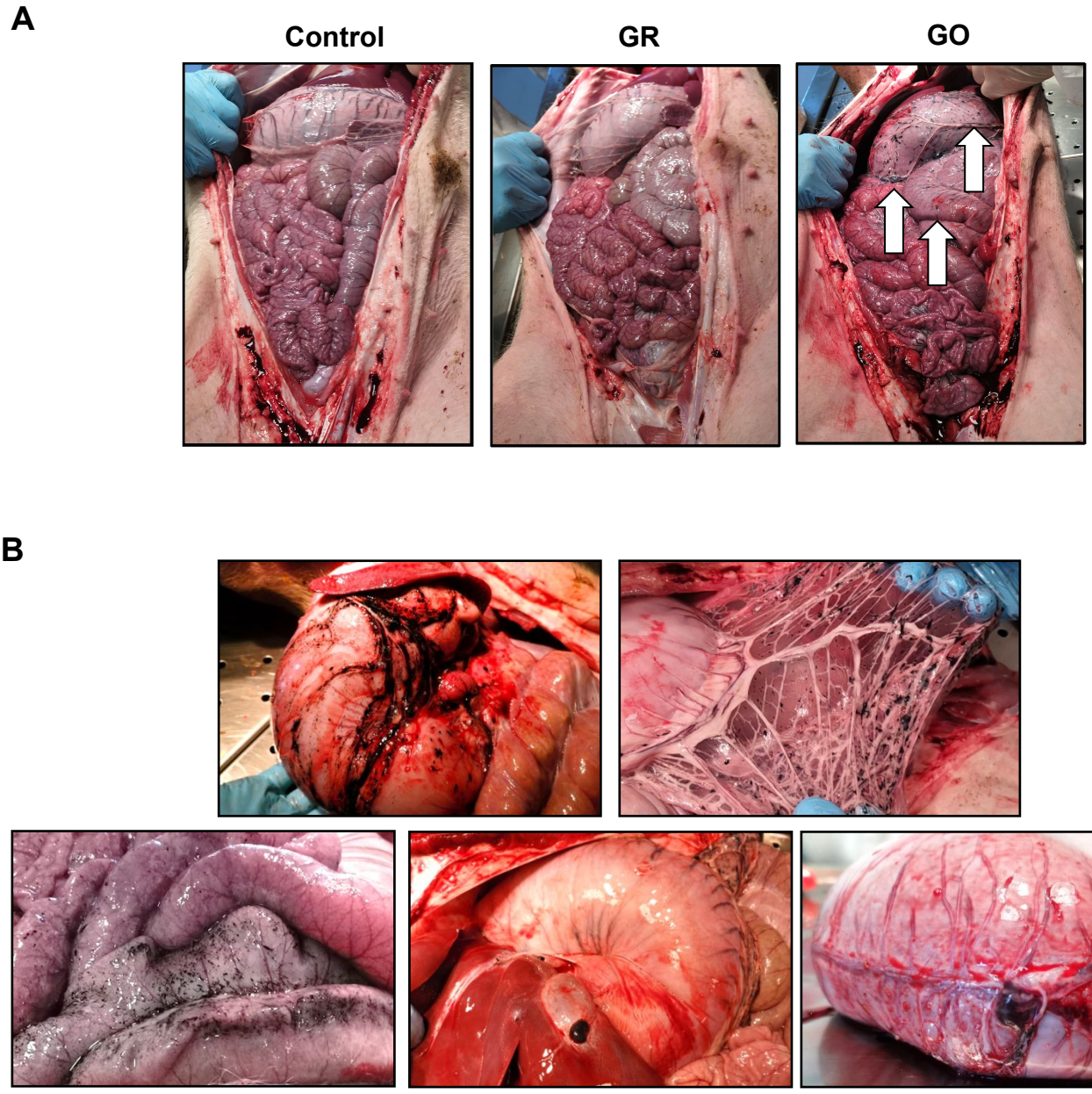

Figure S9. General view of dissected swine abdominal cavity and GO distribution in diverse organs. Pigs were injected intra-peritoneally with 15 mg of GR or GO or water, all with glucose (final glucose 5% w/v) and 21 days later were sacrificed. A) Autopsy was performed and a general view of the abdominal cavity of three representative pigs is reported. Visible nanoparticle aggregates in mesentery are visible in GO treated pigs. B) Representative images of abdominal cavity organs of GO tested subject (#02, #14, #07, #04, #06) are shown.

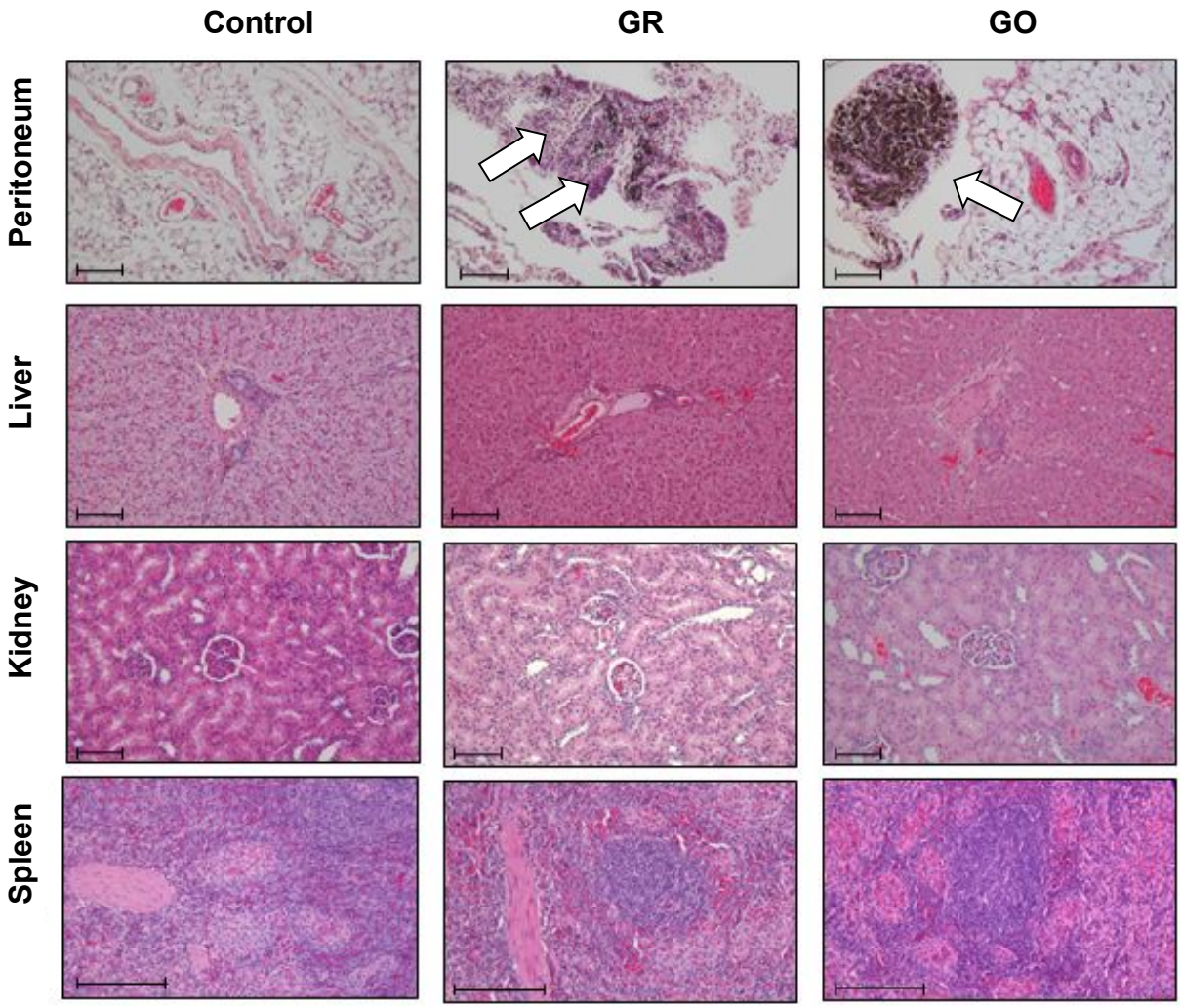

Figure S10. H&E staining. Pigs were injected intra-peritoneally with 15 mg of GR or GO or water, all with glucose (final glucose 5% w/v) and 21 days later were sacrificed. Autopsy was performed and H&E were performed on paraffin-embedded sections of peritoneum, liver, spleen and kidney collected 21 days from GR or GO injection. Images of three representative pigs, one from each group (control, GR, GO) are displayed. Scale bar, 100 μm.

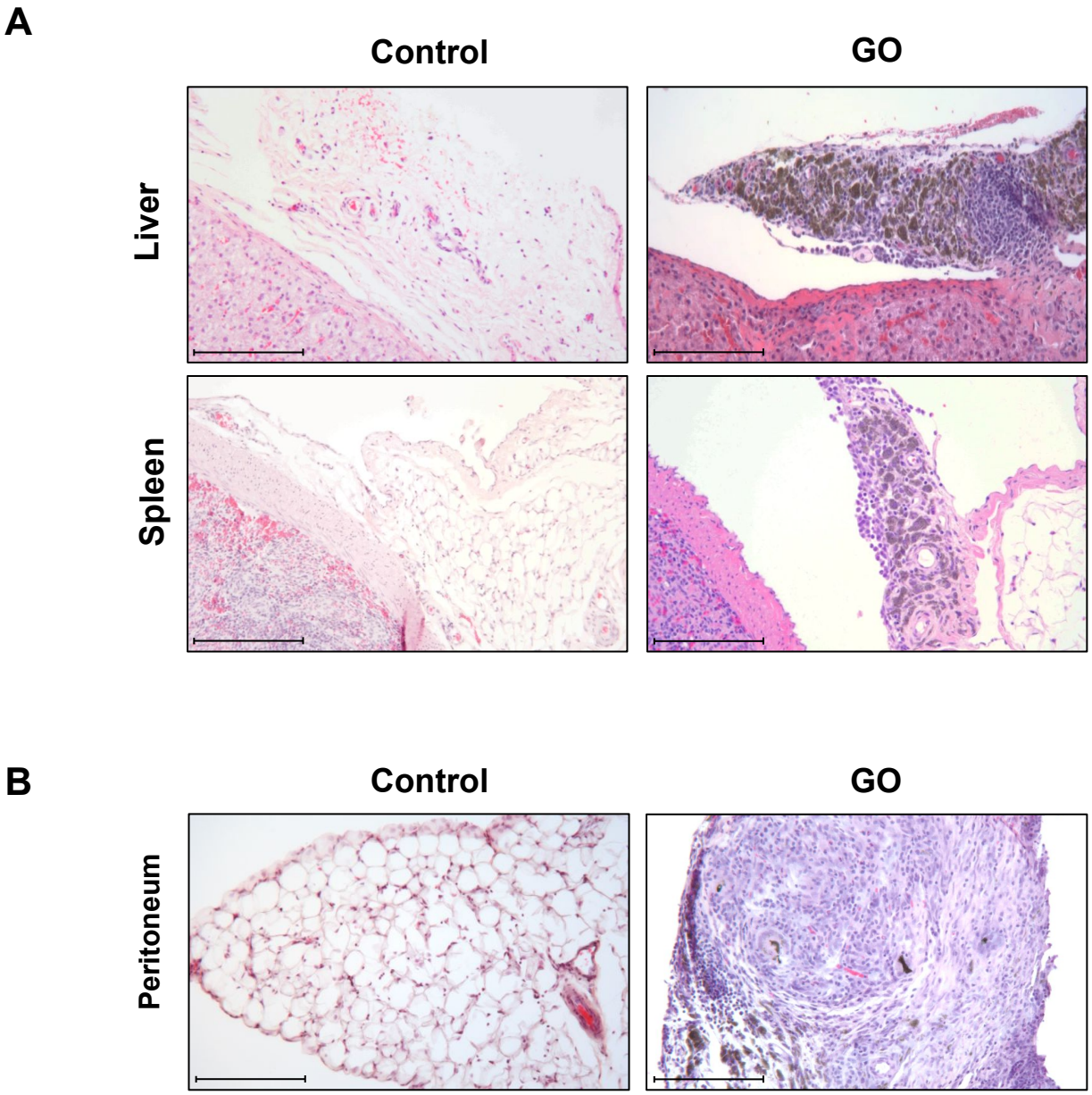

Figure S11. GBM distribution in treated subjects. Pigs were injected intra-peritoneally with 15 mg of GR or GO or water, all with glucose (final glucose 5% w/v) and 21 days later were sacrificed. Autopsy was performed and H&E were performed on paraffin-embedded sections of liver and spleen (panel A) or mesentery (panel B). A) GO aggregates are visible in the serosa but not in the parenchyma of liver and spleen. Representative images of control (#10) and a GO tested subject (#04) are displayed. White arrows indicate GBMs-aggregates. B) H&E staining of mesentery of a control (#10) and a GO tested subject (#06). White arrows indicate GBMs-aggregates within giant cells. For panel A, B, scale bar, 100 μm.

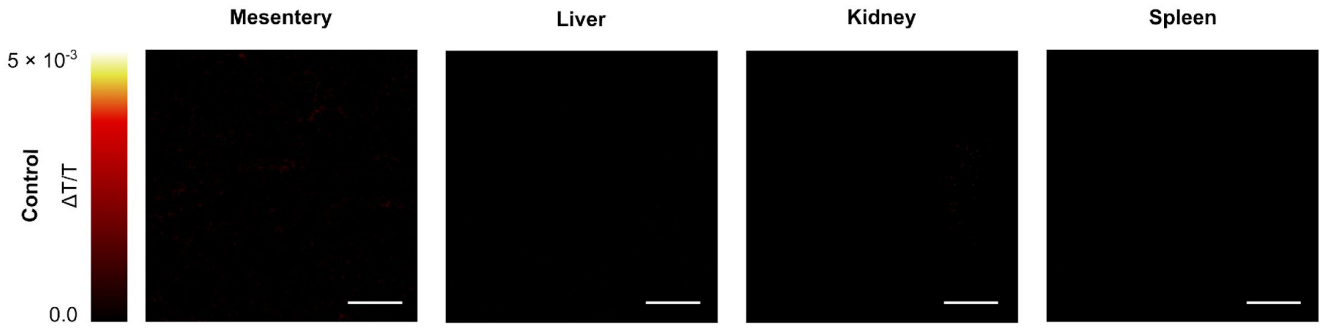

Figure S12. TA imaging on control animals. Pigs were injected intra-peritoneally with water containing glucose (final glucose 5% w/v) and 21 days later were sacrificed. TA imaging was carried out on paraffin-embedded sections of peritoneum, liver, spleen and kidney collected 21 days from control group. Representative TA images related to organs extracted from control animal are displayed. Scale bars: 50 μm.

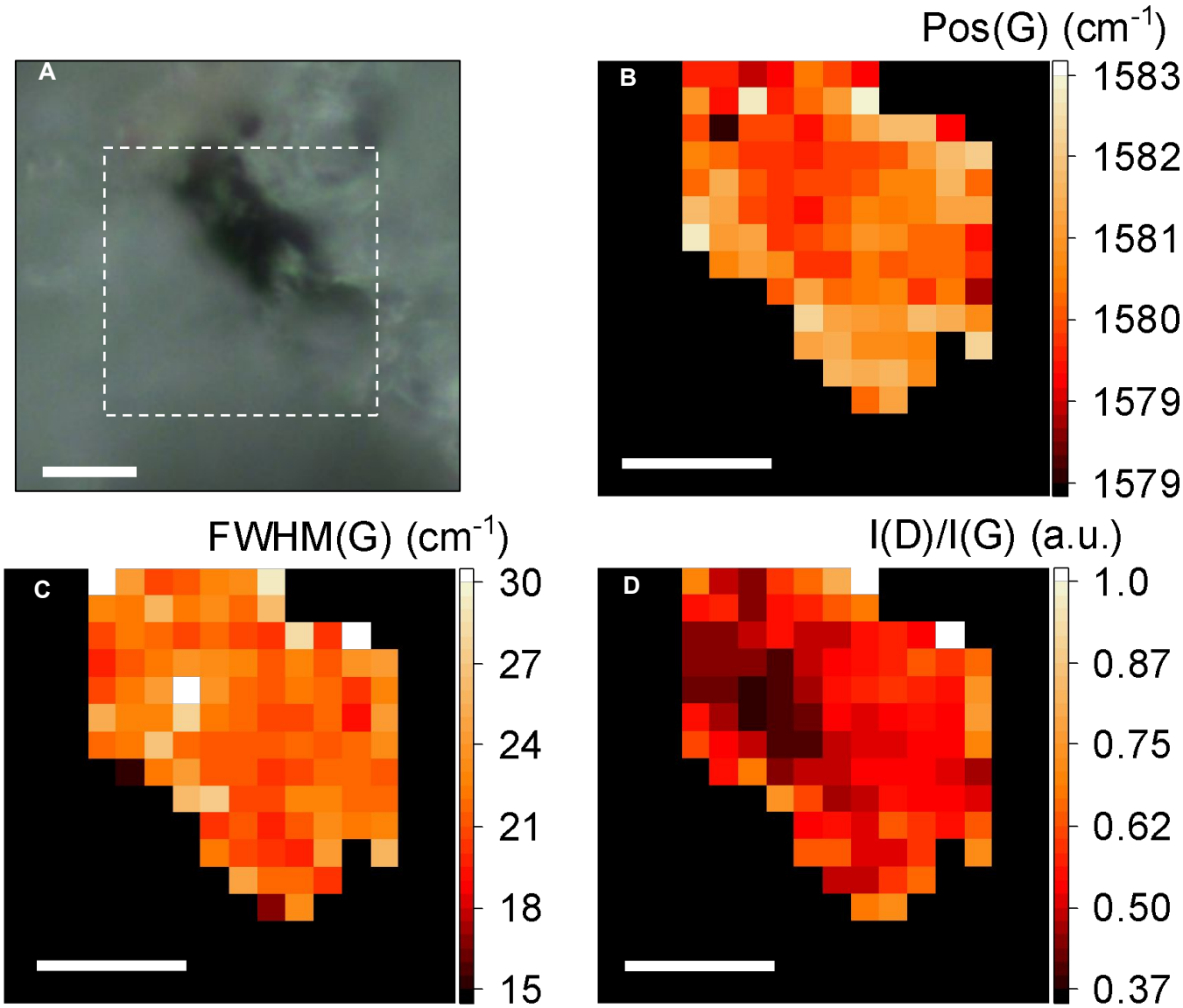

Figure S13. Raman imaging of GR-treated mesentery tissue. A) An optical micrograph of the sample is presented. The dashed rectangle indicates one of the regions where confocal Raman mapping was performed. B) ,C) and D) Areal maps of Pos(*G*), FWHM(*G*), and *I*(*D*)/*I*(*G*), respectively, are presented. The scale bar is 5 μm in all the panels.

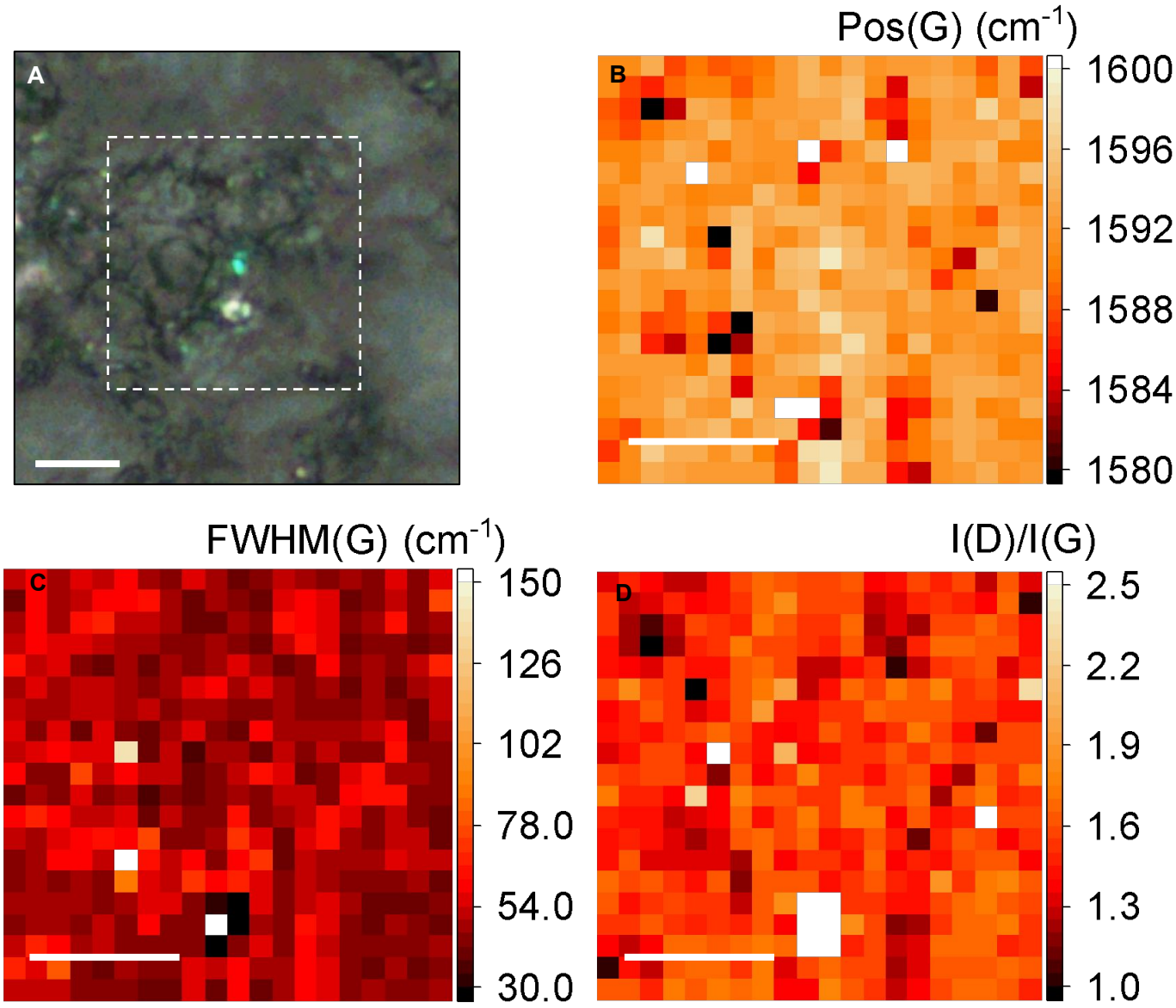

Figure S14. Raman imaging of GO-treated mesentery tissue. A) An optical micrograph of the GO-treated mesentery sample is presented. The dashed rectangle indicates one of the regions where confocal Raman mapping was performed. B) ,C) and D) Areal maps of Pos(*G*), FWHM(*G*), and *I*(*D*)/*I*(*G*), respectively, are presented. The scale bar is 5 μm in all the panels.

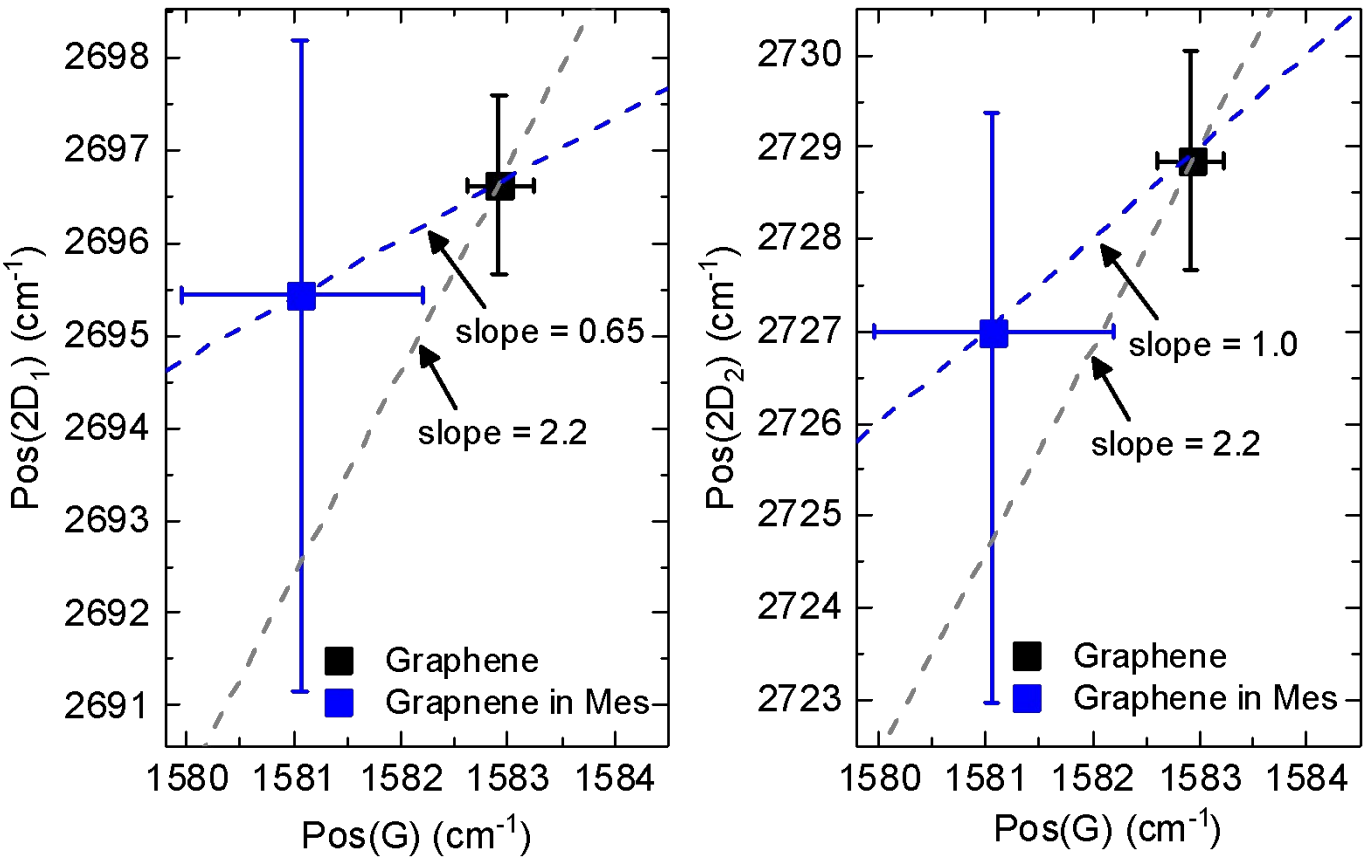

Figure S15. Raman analysis of Pos(2D) vs Pos(G). The mode values of the Pos($2D_1$) Pos($2D_2$) and Pos (G) from the control graphene (black data points) and graphene in mesentery (blue data points), are presented. A) and B) show the Pos($2D_1$) vs Pos (G), and Pos($2D_2$) vs Pos (G) data, respectively, before and after injection. The slopes of the blue dashed lines indicate the observed ΔPos($2D_1$)/ΔPos(G) and ΔPos($2D_2$)/ΔPos(G). The slope of the grey dashed lines indicate the expected ΔPos($2D$)/ΔPos(G) in the case of strain induced shifts.

Table S1. List for pigs used in the *in vivo* experiment.

Treatment	Pig number	Gender
Control	#10	Male
	#11	Male
	#12	Female
GR	#01	Female
	#03	Male
	#08	Male
	#09	Male
	#13	Male
GO	#02	Male
	#04	Male
	#06	Male
	#07	Female
	#14	Female

Table S2. List of biochemical, electrophoretic, and haematological parameters evaluated during the study, indicated as abbreviation (unit of measure) and laboratory reference ranges in healthy pigs.

Parameters (abbreviation)	Unit of measure	Reference range
Alkaline phosphatase (ALP)	[U/L]	20 – 250
Total Bilirubin	[mg/dL]	0 – 0.24
Calcium	[mg/dL]	10 – 11.5
Creatinine	[mg/dL]	0 – 2.5
Phosphorus	[mg/dL]	6.5 -10.2
Total Proteins	[g/dL]	6 – 8.5
Gamma-glutamyl transpeptidase (GGT)	[U/L]	4 – 37
Aspartate aminotransferase (AST/GOT)	[U/L]	0 – 22
Blood urea nitrogen (UREA)	[mg/dL]	17 – 48
Cholesterol	[mg/dL]	80 – 230
Creatine phosphokinase (CPK)	[U/L]	0 – 500
Trigliceride	[mg/dL]	60 – 105
White blood cells (WBC)	[10^3/µL]	11.3 – 22.8
Red blood cells (RBC)	[10^6/µL]	5.9 – 8.8
Hematocrit (HCT)	%	31.1 – 45.9
Hemoglobin	[g/dL]	10.1 – 15.1
Mean corpuscular hemoglobin (MCH)	[pg]	14.4 – 20.1
Mean corpuscular hemoglobin concentration (MCHC)	[g/dL]	30.6 – 34.4
Platelets	[10^3/µL]	138.2 – 467.8
Red blood cells distribution width (RDW)	[%]	14.8 – 19.8
Hemoglobin distribution width (HDW)	[g/dL]	1.4 – 2.3
Total number of neutrophils	[10^3/µL]	3.1 – 9.6
Total number of lymphocytes	[10^3/µL]	4.6 – 10
Total number of monocytes	[10^3/µL]	0.3 – 1.2
Albumin	[%]	40-52
ALFA1 globulins	[%]	5.7 – 6.6
BETA globulins	[%]	12.1 – 16.1
GAMMA globulins	[%]	15.2 – 23.8

Unit of measure: %, percentage; g/dL, grams per decilitre; mg/dL, milligram per decilitre; pg, picogram; fL, femtoliter; U/L, units per litre; 10^3/µL, 10^3 per microlitre; 10^6/µL, 10^6 per microliter.

Table S3. List of analyzed genes.

Position	UniGene	GenBank	Symbol	Description
A01	Ssc.78659	NM_214370	ADIPOQ	Adiponectin, C1Q and collagen domain containing
A02	Ssc.56768	NM_001114283	AIMP1	Aminoacyl tRNA synthetase complex-interacting multifunctional protein 1
A03	Ssc.54377	XM_001927773	BMP1	Bone morphogenetic protein 1
A04	N/A	XM_003125070	BMP10	Bone morphogenetic protein 10
A05	Ssc.4190	NM_001195399	BMP2	Bone morphogenetic protein 2
A06	Ssc.33398	NM_001206388	BMP3	Bone morphogenetic protein 3
A07	Ssc.16690	NM_001101031	BMP4	Bone morphogenetic protein 4
A08	Ssc.66621	NM_001204901	BMP5	Bone morphogenetic protein 5
A09	Ssc.66765	NM_001168001	BMP6	Bone morphogenetic protein 6
A10	Ssc.21774	NM_001105290	BMP7	Bone morphogenetic protein 7
A11	Ssc.21108	NM_001001646	C5	Complement component 5
A12	Ssc.15861	NM_214126	CD40LG	CD40 ligand
B01	Ssc.42649	NM_001044531	CD70	CD70 molecule
B02	Ssc.382	NM_214118	CSF2	Colony stimulating factor 2 (granulocyte-macrophage)
B03	Ssc.16151	NM_213842	CSF3	Colony stimulating factor 3 (granulocyte)
B04	N/A	XM_003132779	FAM3B	Family with sequence similarity 3, member B
B05	Ssc.15870	NM_213806	FASLG	Fas ligand (TNF superfamily, member 6)
B06	N/A	XM_003133924	FGF10	Fibroblast growth factor 10
B07	N/A	XM_001928382	FIGF	C-fos induced growth factor (vascular endothelial growth factor D)
B08	Ssc.43123	NM_001174056	GDF15	Growth differentiation factor 15
B09	N/A	XM_003133104	GDF2	Growth differentiation factor 2
B10	Ssc.28726	NM_001244297	GDF5	Growth differentiation factor 5
B11	Ssc.20042	NM_001001909	GDF9	Growth differentiation factor 9
B12	Ssc.95872	NM_001164860	IFN-ALPHA-5	Interferon, alpha 5
C01	Ssc.42778	NM_001003923	IFNB1	Interferon beta
C02	Ssc.4093	NM_213948	IFNG	Interferon-gamma
C03	Ssc.148	NM_214041	IL10	Interleukin 10
C04	Ssc.13	NM_213993	IL12A	Interleukin 12A (natural killer cell stimulatory factor 1, cytotoxic lymphocyte maturation factor 1, p35)
C05	Ssc.71	NM_214013	IL12B	Interleukin 12B (natural killer cell stimulatory factor 2, cytotoxic lymphocyte maturation factor 2, p40)
C06	Ssc.15877	NM_213803	IL13	Interleukin 13
C07	Ssc.8833	NM_214390	IL15	Interleukin 15
C08	Ssc.18652	NM_213751	IL16	Interleukin 16
C09	Ssc.42770	NM_001005729	IL17A	Interleukin 17A
C10	Ssc.51662	XM_001924366	IL17F	Interleukin 17F
C11	Ssc.20	NM_213997	IL18	Interleukin 18 (interferon-gamma-inducing factor)
C12	Ssc.51659	XM_003130464	IL19	Interleukin 19
D01	Ssc.113	NM_214029	IL1A	Interleukin 1, alpha
D02	Ssc.28829	NM_214055	IL1B	Interleukin 1, beta
D03	Ssc.16250	NM_214262	IL1RN	Interleukin 1 receptor antagonist
D04	Ssc.16224	NM_213861	IL2	Interleukin 2
D05	Ssc.26323	NM_214415	IL21	Interleukin 21
D06	Ssc.42733	XM_001926156	IL22	Interleukin 22
D07	Ssc.56047	NM_001130236	IL23A	Interleukin 23, alpha subunit p19
D08	Ssc.75345	XM_005666258	IL25	Interleukin 25
D09	Ssc.36782	NM_001007520	IL27	Interleukin 27
D10	Ssc.15837	NM_214123	IL4	Interleukin 4
D11	Ssc.528	NM_214205	IL5	Interleukin 5
D12	Ssc.62	NM_214399	IL6	Interleukin 6 (interferon, beta 2)

E01	Ssc.15904	NM_214135	IL7	Interleukin 7
E02	Ssc.51687	NM_001166043	IL9	Interleukin 9
E03	Ssc.18993	NM_214189	INHA	Inhibin, alpha
E04	Ssc.52080	NM_214028	INHBA	Inhibin, beta A
E05	Ssc.16230	NM_001164842	INHBB	Inhibin, beta B
E06	Ssc.52878	NM_214402	LIF	Leukemia inhibitory factor (cholinergic differentiation factor)
E07	N/A	XM_001929161	OSM	Oncostatin-M-like
E08	N/A	XM_003124086	IL17B	Interleukin-17B-like
E09	N/A	XM_003123626	SCGB3A1	Secretoglobin family 3A member 1-like
E10	Ssc.51664	XM_003130310	LOC100037931	Tumor necrosis factor superfamily member 18
E11	N/A	XM_003122707	CNTF	Ciliary neurotrophic factor-like
E12	Ssc.102621	NM_001260482	LOC100519468	Tumor necrosis factor ligand superfamily member 14-like
F01	N/A	XM_003124238	PDGFA	Platelet-derived growth factor alpha polypeptide
F02	N/A	XM_003130465	IL20	Interleukin-20-like
F03	N/A	XM_003130670	IL11RA	Interleukin-11 receptor subunit alpha-like
F04	N/A	XM_003483282	THPO	Thrombopoietin
F05	N/A	XR_305507	LOC100621682	Uncharacterized LOC100621682
F06	N/A	XM_003480815	TNFSF9	Tumor necrosis factor ligand superfamily member 9-like
F07	Ssc.27595	NM_214453	LTA	Lymphotoxin alpha (TNF superfamily, member 1)
F08	Ssc.15277	NM_001185138	LTB	Lymphotoxin beta (TNF superfamily, member 3)
F09	Ssc.551	NM_001077213	MIF	Macrophage migration inhibitory factor (glycosylation-inhibiting factor)
F10	Ssc.23498	NM_214435	MSTN	Myostatin
F11	Ssc.22083	NM_001031793	NAMPT	Nicotinamide phosphoribosyltransferase
F12	Ssc.23321	NM_214023	SPP1	Secreted phosphoprotein 1
G01	Ssc.94427	NM_214251	TGFA	Transforming growth factor, alpha
G02	Ssc.76	NM_214015	TGFB1	Transforming growth factor, beta 1
G03	Ssc.10287	XM_005653762	TGFB2	Transforming growth factor, beta 2
G04	Ssc.27593	NM_214198	TGFB3	Transforming growth factor, beta 3
G05	Ssc.100	NM_214022	TNF	Tumor necrosis factor
G06	Ssc.90180	XM_003481346	TNFRSF11B	Tumor necrosis factor receptor superfamily, member 11b
G07	Ssc.12829	NM_001024696	TNFSF10	Tumor necrosis factor (ligand) superfamily, member 10
G08	Ssc.47270	NM_001097498	TNFSF13B	Tumor necrosis factor (ligand) superfamily, member 13b
G09	Ssc.73905	NM_001244555	TNFSF15	Tumor necrosis factor (ligand) superfamily, member 15
G10	Ssc.23487	NM_001025217	TNFSF4	Tumor necrosis factor (ligand) superfamily, member 4
G11	Ssc.70020	XM_003127774	TXLNA	Taxilin alpha
G12	Ssc.57541	NM_214084	VEGFA	Vascular endothelial growth factor A
H01	Ssc.10316	XM_003357928	ACTB	Actin, beta
H02	Ssc.73773	NM_213978	B2M	Beta-2-microglobulin
H03	Ssc.79971	NM_001206359	GAPDH	Glyceraldehyde-3-phosphate dehydrogenase
H04	Ssc.4158	NM_001032376	HPRT1	Hypoxanthine phosphoribosyltransferase 1
H05	Ssc.17024	NM_001244068	RPL13A	Ribosomal protein L13a
H06	N/A	SA_00133	SGDC	Pig Genomic DNA Contamination
H07	N/A	SA_00104	RTC	Reverse Transcription Control
H08	N/A	SA_00104	RTC	Reverse Transcription Control
H09	N/A	SA_00104	RTC	Reverse Transcription Control
H10	N/A	SA_00103	PPC	Positive PCR Control
H11	N/A	SA_00103	PPC	Positive PCR Control
H12	N/A	SA_00103	PPC	Positive PCR Control

Table S4. List of genes significantly up or down-regulated in vehicle control group. If fold change > 1, fold regulation = fold change; if fold change < 1, fold regulation = -1/fold change.

Gene	Fold regulation	p-value
ADIPOQ	2.69	0.048263
TXLNA	2.09	0.023664
THPO	2.07	0.032335
TNFSF14	1.36	0.014442
IL16	1.43	0.029694
GDF2	-1.30	0.047257
GDF5	-1.20	0.015059
IL19	-1.19	0.021798

Table S5. List of genes significantly up or down-regulated at T1 in graphene pristine (GR) and GO groups compared to vehicle controls. If fold change > 1, fold regulation = fold change; if fold change < 1, fold regulation = -1/fold change.

	Gene	Fold regulation	p-value
GR_T1/Control_T1	IL1A	2.17	0.012473
	FASLG	-1.74	0.010014
GO_T1/Control_T1	IL21	2.87	0.000621
	LTB	1.58	0.038063
	BMP2	1.56	0.000898
	AIMP1	1.35	0.015272
	IL16	1.11	0.039959